Journal of Marine Science and Technology

Volume 22 | Issue 4 Article 10

BEHAVIORS OF LARGE-SCALE DRIVEN PC PILES

Shih-Tsung Hsu
Department of Construction Engineering, Chaoyang University of Technology, Taichung, Taiwan, R.O.C,
sthsu@cyut.edu.tw

Recommended Citation

Hsu, Shih-Tsung (2014) "BEHAVIORS OF LARGE-SCALE DRIVEN PC PILES," *Journal of Marine Science and Technology*: Vol. 22: Iss. 4, Article 10.
DOI: 10.6119/JMST-013-0606-3
Available at: https://jmstt.ntou.edu.tw/journal/vol22/iss4/10

BEHAVIORS OF LARGE-SCALE DRIVEN PC PILES

Acknowledgements

The authors would like to thank the National Science Council of the Republic of China, Taiwan, for financially supporting this research under Grant No. NSC 99-2628-E324-005. The authors also appreciate Professor Hwang, J. H. of National Central University, Professor Chen, C. H. of National Taiwan University, and Mr. Yeh, W. C. of Resources Engineering Services Inc., for providing a tremendous amount of information on pile driving, and Mr. Hung, C. J., and Mr. Chen, C. K., of Da-Chen Construction and Engineering Corp. for helping with the installation and testing of the test piles.

Journal of Marine Science and Technology, Vol. 22, No. 4, pp. 487-497 (2014)
DOI: 10.6119/JMST-013-0606-3

BEHAVIORS OF LARGE-SCALE DRIVEN PC PILES

Shih-Tsung Hsu

Key words: driven pile, residual load, ultimate load, ground movement.

ABSTRACT

This study developed a numerical method for evaluating ground movements while a pile is being driven and obtained a comprehensive load-displacement curve for a driven pile. The tested pile exhibited a larger scale than those tested in previous studies, and was penetrated into a considerable depth of the stratum.

Numerical results revealed that both the ground movement and residual force caused by the pile driving was able to be analyzed using the proposed numerical procedure. Although the load applied to the tested piles differed from that determined by numerically analyzing incremental pile displacement, the load-displacement behavior of the piles calculated using the proposed method was consistent with that measured in pile-load tests before the piles were stressed to their peak loads. This study presents a series of helpful figures to support the design of driven precast concrete piles based on the results of numerical studies and field tests.

I. INTRODUCTION

Driven precast piles are usually used along the banks of rivers in urban districts, such as the Keelung River in the Taipei Basin. Heavy industries are commonly located on the outskirts of population centers, such as the western coast of Taiwan, where the land is formed by filling with reclaimed soil. The bank and reclaimed site suffer from problems of bearing capacity and settlement. Using piles can help solve construction problems in these areas.

Because reclaimed land is usually far from urban regions, the noise and vibration created by driving piles are acceptable. Driven piles are typically adopted as deep foundations for most factory buildings in many industrial parks in Taiwan, where a precast concrete (PC) pile with a closed end commonly serves as a driven pile. This type of pile typically has a diameter of approximately 50 or 60 cm, and can be as large as 100 cm. A PC pile is normally less than 35 m in length.

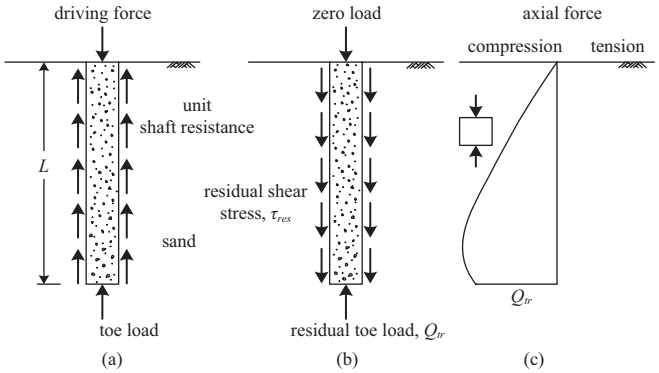

Fig. 1. Residual load induced by driving a pile (Alawneh *et al.* [1]).

The ultimate pile capacity, Q_u, is generally a combination of the ultimate shaft friction, Q_s, and the ultimate point bearing, Q_p. However, Burland [6] indicated that the total load, shaft friction, and point bearing do not reach their peaks simultaneously. When the shaft friction reaches its maximum value, the point bearing is still small; when the point bearing is at its maximum value, the shaft friction is at its residual value. Furthermore, if punching shear failure occurs under the pile base, the point bearing has no peak value.

Briaud and Tucker [5] proposed the concept of residual force for a pile being driven. Fig. 1 is the schematic diagram of a residual load [1]. For a pile during placement, shaft friction and toe load are generated against the driving force (Fig. 1(a)). After removing the driving force, the pile rebounds elastically, resulting in residual shear stress along the pile shaft and a residual toe load beneath the pile base (Fig. 1(b)). Fig. 1(c) illustrates the axial force along a pile shaft after removing the driving force.

Researchers have investigated pile behaviors through field tests, model tests, numerical methods, and experimental formulas established according to the pile database. Mansur and Hunter [21] recorded load-displacement relationships and presented design charts after performing many pile tests along the Arkansas River. Altaee *et al*. [2] drove a PC pile equipped with strain gauges (11.0 m) into a sandy deposit, and measured

Paper submitted 06/27/12; revised 03/26/13; accepted 06/06/13. Author for correspondence: Shih-Tsung Hsu (e-mail: sthsu@cyut.edu.tw).
Department of Construction Engineering, Chaoyang University of Technology, Taichung, Taiwan, R.O.C.

Table 1. Properties of sand in triaxial test.

Effective size, D_{10} (mm)	Diameter corresponding to 30% finer, D_{30} (mm)	Diameter corresponding to 60% finer, D_{60} (mm)	Coefficient of uniformity, C_c	Coefficient of gradation, C_g
0.11	0.33	0.45	4.09	2.2

Fines content (%)	Soil type	Specific gravity, *Gs*	Maximum dry density, $\gamma_{d,\,max}$ (kN/m^3)	Minimum dry density, $\gamma_{d,\,min}$ (kN/m^3)
13	*SM* (Silty Sand)	2.69	15.78	13.69

the load-displacement and loads imposed on the pile body and residual force as the pile was stressed. Altaee *et al*. [3] also presented the results of numerically simulating driven piles, and concluded that no critical depth can be found for driven piles when using the nonlinear finite element method. Nevertheless, the numerical method could not accurately estimate the peak load of a driven pile or assess the post-peak behavior. Briaud and Tucker [5] devised a calculated method based on a simple theory and on a 33 database that can reasonably predict the behavior of Arkansas River Pile 1 [21]. However, the pile dimensions that have appeared in most previous studies are small: the pile diameter ranges from 28 cm to 46 cm, and the pile length is 3-18 m [1, 2].

Engineers in Taiwan have accumulated substantial experience in constructing and field testing driven PC piles. Chen *et al*. [8] discussed the relationship between ultimate loads and yielding loads of driven PC piles. Because most pile load tests adopt the incremental load method, the load-displacement curve does not reach its real peak; therefore, the ultimate pile capacity cannot be estimated accurately. In addition, tested piles are rarely stressed to failure; thus, a comprehensive load-displacement curve cannot be obtained. If the pile base does not have a load cell to measure the point bearing, then an empirical technique should be used to separate the shaft friction from the point bearing on the load-displacement curve [8].

Because of the variability of strata and the unknown reliability of construction techniques, numerous tests must be conducted to evaluate the behaviors of piles accurately. Therefore, researchers often adopt numerical methods to analyze pile behavior [14, 15]. The soil model is assumed to be an elastic-perfectly plastic model [22, 24, 26] and, similar to the strain hardening model [10], typically neglects the behavior of strain softening and volumetric dilation in sand. These models can accurately predict piles pre-peak, but not post-peak. However, a complete and accurate load-displacement curve of a pile cannot be obtained if the strain-softening behavior of soil is not considered.

These situations require using a numerical method that can obtain precise analytical results of the total load, shaft friction, and point bearing against the displacement of a driven PC pile. Such a model could accurately estimate the relationships of ultimate load versus pile length, pile diameter, and shear strength of the soil.

Hsu and Liao [16] developed a constitutive model for continuous strain hardening-softening and the volumetric dilation of cohesionless soils. Lin [20] created a model for continuous strain hardening-softening of undrained clay. Hsu, *et al*. [17] successfully analyzed behaviors of prestressed concrete piles when adopting both of these two model; therefore, the current study adopted the models to simulate ground movements during the driving of a pile, analyzed the residual load induced by the driving of a pile, and finally, examined the behavior of axially loaded driven piles in sandy soil. This study compared the numerical results with the measured test results from current and previous studies, and parametrically analyzed the factors affecting the behavior of driven piles.

II. STRESS-STRAIN BEHAVIORS OF SOILS

Hwang *et al*. [18] conducted a series of pile tests in the Chiayi-Taibao City in Taiwan. All piles were driven into alluvial soil, which consists of alternating layers of sand and clay. This study simulated a part of their measurements. Therefore, introducing the constitutive models for sand and clay is required.

Table 1 shows the properties of the sand specimen, which was used in triaxial tests. To model the stress-strain behavior of sand, this study adopted the constitutive model developed by Hsu and Liao [16], based on plasticity theory and the non-associated flow rule. The yield function *f* is

$$f = \sigma_1^{'} - \sigma_3^{'} \frac{1+\sin\phi^*}{1-\sin\phi^*} \tag{1}$$

where $\sigma_1^{'}$ represents the effective major principal stress, $\sigma_3^{'}$ is the effective minor principal stress, and ϕ^* is the mobilized friction angle, which is a function of the accumulative plastic strain ε^p. Because a non-associated flow rule was adopted, a plastic potential function g was required to describe the relationship between the plastic strain increment $d\varepsilon_{ij}^p$ and the effective stress tensor $\sigma_{ij}^{'}$. The plastic potential function *g* can be expressed as

$$g = \sigma_1^{'} - \sigma_3^{'} \frac{1+\sin\psi^*}{1-\sin\psi^*} \tag{2}$$

where ψ^* is the mobilized dilatancy angle, which is also a function of the accumulative plastic strain ε^p. Table 2 presents

Table 2. Parameters of sand (Partial information from Hsu and Liao [16]).

Parameters	Equations
Elastic modulus, E	$E = 500 \times D_r \times P_a \times \left(\frac{\sigma_3}{P_a}\right)^{0.5}$
Bulk modulus, B	$B = (22 + 165 D_r) \times P_a \times \left(\frac{\sigma_3}{P_a}\right)^{0.2}$
Accumulative plastic strain, ε_p	$\varepsilon_p = \left(\varepsilon_a^p - \frac{1}{3}\varepsilon_v^p\right) = \left(\varepsilon_a - \frac{1}{3}\varepsilon_v\right) - \left(\varepsilon_a^e - \frac{1}{3}\varepsilon_v^e\right)$
Accumulative plastic strain at peak deviator stress, ε_p^f	$\varepsilon_p^f = \frac{(10 - 7.78 D_r)}{100} \times (\frac{\sigma_3}{P_a})^{0.6}$
Strain softening parameter, ε_p^c	$\varepsilon_p^c = \left(\frac{20 - 10 \times D_r}{100}\right)$
Mobilized friction angle, ϕ^*	$0 < \varepsilon_p < \varepsilon_p^f$ $\phi^* = \sin^{-1}\left(\frac{2\sqrt{\varepsilon_p \cdot \varepsilon_p^f}}{\varepsilon_p + \varepsilon_p^f} \times \sin\phi_p\right)$ $\varepsilon_p > \varepsilon_p^f$ $\phi^* = \phi_{cv} + (\phi_p - \phi_{cv}) \times \exp\left[-\left(\frac{\varepsilon_p - \varepsilon_p^f}{\varepsilon_p^c}\right)^2\right]$
Peak friction angle, ϕ_p	$\phi_p = 32 + 10 D_r - (2.5 + 8 D_r) \times \log\left(\frac{\sigma_3}{P_a}\right)$
Constant volume friction angle, ϕ_{cv}	$\phi_{cv} = 32^\circ$
Mobilized dilatancy angle, ψ^*	$\psi^* = \sin^{-1}\left(\frac{\sin\phi^* - \sin\theta}{1 - \sin\phi^* \times \sin\theta}\right)$
Dilatancy parameter, θ	$0 < \varepsilon_p < \varepsilon_p^d, \theta = \phi^*$ $\varepsilon_p^d < \varepsilon_p < \varepsilon_p^f,$ $\theta = \phi_d + (\phi_{cv} - \phi_d) \times \frac{2\sqrt{(\varepsilon_p - \varepsilon_p^d) \times (\varepsilon_p^f - \varepsilon_p^d)}}{(\varepsilon_p - \varepsilon_p^d) + (\varepsilon_p^f - \varepsilon_p^d)}$ $\varepsilon_p > \varepsilon_p^f, \theta = \phi_{cv}$
Accumulative plastic strain at initial dilatancy, ε_p^d	$\varepsilon_p^d = \frac{(8.6 - 10.15 D_r)}{100} \times \left(\frac{\sigma_3}{P_a}\right)^{2.2}$
Mobilized friction angle at initial dilatancy, ϕ_d	$\phi_d = \sin^{-1}\left(\frac{2\sqrt{\varepsilon_p^d \times \varepsilon_p^f}}{\varepsilon_p^d + \varepsilon_p^f} \times \sin\phi_p\right)$

the constitutive equations and the related parameters of silty sand. To demonstrate the reliability of this constitutive model, the stress-strain behaviors of silty sand with a relative density of 70%, determined from the triaxial test were compared with those calculated using the proposed model. As Fig. 2 illustrates, the calculated results are perfectly consistent with the triaxial test results. Hsu [13] provided a detailed illustration of this model.

Table 3. Properties of clay in triaxial test.

Liquid Limit, *LL*	Plasticity index, *PI*	Soil type	Water content, ω_n(%)	Specific gravity, G_s	Unit weight, γ_t(kN/m^3)
41	18	*CL* (Lean clay)	42	2.72	18.6

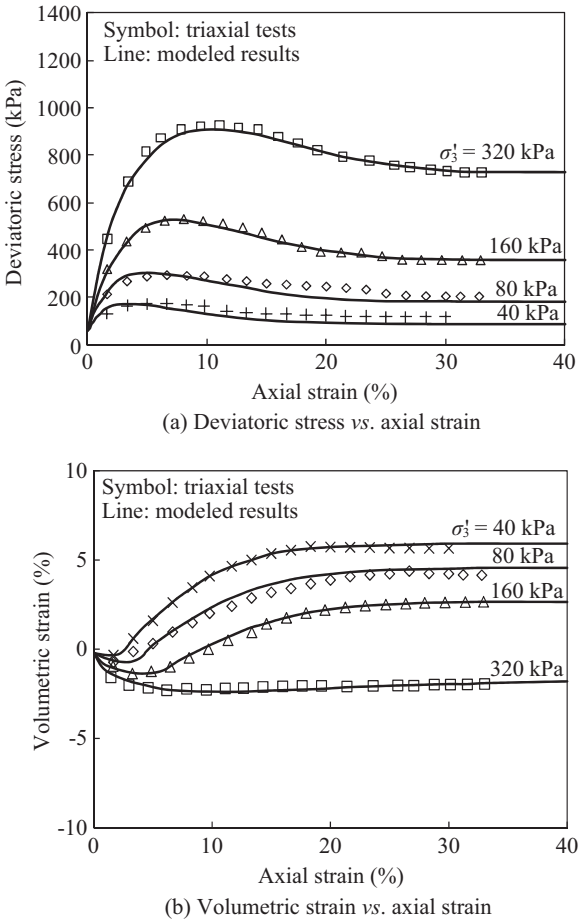

Fig. 2. Comparison of measured and modeled stress-strain behavior of sand with relative density D_r of 70%.

Table 3 shows the properties of the clay that was used in the triaxial test. This study adopted the constitutive model of clay created by Lin [20] to obtain the parameters required for numerical analysis. Because the clay was assumed to be undrained, the yield function f is equal to the plastic potential function g, and can be represented as

$$f = g = \sigma_1 - \sigma_3 - 2S_u^* \tag{3}$$

Table 4. Parameters of clay (Partial information from Lin [20]).

Parameters	Equations
Elastic modulus, E	$E = 700 \times S_u$
Accumulative plastic strain at peak deviator stress, ε_p^f	$\varepsilon_p^f = 0.04 \times (\frac{S_u}{P_a})^{0.9}$
Strain softening parameter, ε_p^c	$\varepsilon_p^c = 0.1 \times (\frac{S_u}{P_a})$
Residual undrained shear strength, S_{ur}	$S_{ur} = 0.8 \times S_u$
Mobilized undrained shear strength, S_u^*	$0 < \varepsilon_p \le \varepsilon_p^f$, $S_u^* = \frac{2 \times \sqrt{\varepsilon_p \times \varepsilon_p^f}}{\varepsilon_p + \varepsilon_p^f} \times S_u$; $\varepsilon_p > \varepsilon_p^f$, $S_u^* = S_{ur} + (S_u - S_{ur}) \times \exp\left[-(\frac{\varepsilon_p - \varepsilon_p^f}{\varepsilon_p^c})^2\right]$

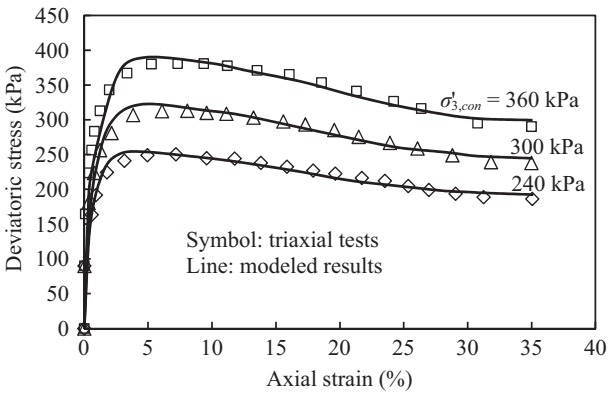

Fig. 3. Comparison of measured and modeled stress-strain behavior of clay.

where σ_1 represents the major principal stress, σ_3 is the minor principal stress, and S_u^* represents the mobilized undrained shear strength, which is related to accumulative plastic strain ε^p. Table 4 presents the constitutive equations and related parameters of clay. To demonstrate the suitability of the constitutive model, the stress-strain behaviors of clay, determined from the triaxial CU test, were compared with those calculated using the proposed model. As Fig. 3 illustrates, the calculated results are perfectly consistent with the triaxial test results. Lin [20] provided more detailed information on this model.

This study analyzed the ground movement of entirely stratum-alternating sand and clay layers when a pile is being driven. However, conducting numerical analyses for estimating load-displacement behavior while a pile was being loaded involved only sandy soil; concurrently, the interface element was used. Desai *et al*. [9] developed an elaborate and suitable interface element for a numerical pile, called the thin-layer element. This study adopted the thin-layer element as the interface element. Desai *et al*. [9] suggested that the thickness t of the interface element is 10 D_{50} to 15 D_{50} (D_{50}: Diameter corresponding to 50% finer); its average equals 12.5 D_{50}. Because D_{50} of sand used in the triaxial test is 0.4 mm, t = 5 mm was adopted in this study for the numerical piles being loaded. The stress-strain behaviors of interfaces were similar to those of the sand element in this study. According to Desai *et al*. [9], the normal stiffness and shear stiffness are $k_n = E/t$ (E: Elastic modulus) and $k_s = G/t$ (G: Shear Modulus), respectively. In this study, the peak friction angle of interface δ equated to ϕ of sand, whereas the residual friction angle of interface δ_r was 26°. Wang [27] described in detail the model parameters. Table 5 presents the constitutive equations and the related parameters of the interface.

Table 5. Parameters of interface (Partial information from Desai *et al*. [9]).

Parameters	Equations	Remarks
Normal stiffness, K_n	$K_n = \frac{E}{t}$	E: Elastic modulus of sand (as shown in Table 2) t: Thickness of the interface element, t = 5 mm
Shear stiffness, K_s	$K_s = \frac{G}{t}$	G: Shear modulus of sand, $G = \frac{3BE}{9B - E}$ B: Bulk modulus of sand (as shown in Table 2)
Accumulative plastic shear strain, γ_p	$\gamma_p = \frac{3}{2}\varepsilon_p$	$\gamma_p = \varepsilon_a^p - \varepsilon_r^p$, $\varepsilon_p = \varepsilon_a^p - \frac{1}{3}\varepsilon_v^p = \varepsilon_a^p - \frac{1}{3}(\varepsilon_a^p + 2\varepsilon_r^p)$ Therefore, $\gamma_p = \frac{3}{2}\varepsilon_p$, ε_p is shown in Table 2
Peak friction angle, ϕ_p	Interface ϕ_p is the same as sand ϕ_p	ϕ_p is shown in Table 2
Constant volume friction angle, ϕ_{cv}	$\phi_{cv} = 26^\circ$	

Note: 1. Because γ_p is equal to $\frac{3}{2}\varepsilon_p$, then the $\gamma_p^f = \frac{3}{2}\varepsilon_p^f$, $\gamma_p^c = \frac{3}{2}\varepsilon_p^c$, and $\gamma_p^d = \frac{3}{2}\varepsilon_p^d$.

2. The parameters ε_p^f, ε_p^c, and ε_p^d are shown in Table 2.

III. GROUND MOVEMENT INDUCED BY A DRIVEN PC PILE

The High-Speed Rail (HSR) in Taiwan passes through the Chiayi-Taibao City. To evaluate the effectiveness of driven PC piles as foundations for an HSR viaduct, Hwang *et al*. [18]

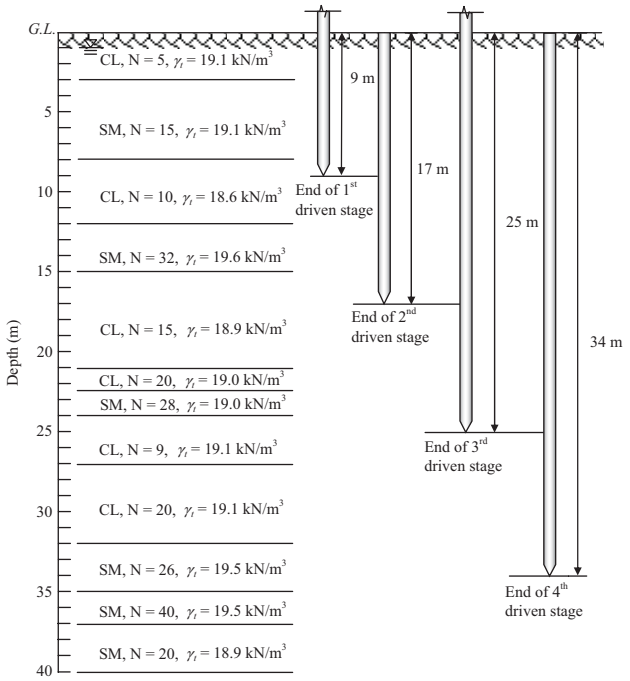

Fig. 4. Subsoil condition and processes of a pile being driven into subsoil of the Chiayi-Taibao City (Redrawn from Hwang *et al.* [18]).

conducted a series of field tests on driven PC piles in Chiayi-Taibao City. They also applied inclinometers, installed at a distance of 3*D* (where *D* is the diameter of a pile) from the center of a pile, to measure the ground movement (radial movement of soil mass) induced by a driven PC pile. This study used their test results to confirm the suitability of the proposed numerical method. The tested pile was composed of precast concrete, with a hollow cross-section, an outer diameter of 80 cm, and an inner diameter of 56 cm. The pile tip was closed and conical. The compressive strength of the concrete was 80 MPa. The pile was precast in two segments, each 17 m in length. During construction, the two segments were driven one after the other and welded end to end to form a total length of 34 m. Because measurements could not be performed using inclinometers as the pile was being driven, measurements were taken only after driving. As Fig. 4 shows, measurements were performed when the PC pile reached designated depths of 9, 17, 25, and 34 m. The pile diameter and the penetrated depth exceeded those recorded in previous studies.

IV. NUMERICAL SIMULATION OF RADIAL GROUND MOVEMENT

Several researchers have simulated pile-driven processes. Holloway *et al*. [12] presented a numerical procedure using a finite difference formulation to simulate the behavior of a pile subjected to one-dimensional impact loading. This procedure enables determining residual stresses induced by the driving. Poulos [23] presented a numerical method for estimating the residual stresses in single piles installed by driving. This method replaces the "dynamic analysis" of Holloway *et al*. [12] by using a "static analysis" to estimate residual load.

Regarding a pushed pile, residual load in the pile caused by the installation is modeled by loading the pile in compression (the pile being at its final embedment depth) until failure and then unloading it back to zero load at its head (Chan and Hanna [7]). Regarding a buried pile, the residual load in the pile is calculated by simulating an incremental accumulation of soil around the pile (Hanna and Tan [11]). However, the residual load of a driven pile is more complex. To simulate the residual load of a driven pile, Altaee *et al*. [3] used the procedure similar to simulating a pushed pile, but with the weight of an upper 1.5-m-thick soil layer excluded from the analysis. Altaee *et al*. [3] demonstrated that numerically analyzed residual loads are close to those measured by conducting a field test.

Because the driven pile behaves axially symmetrically, the three-dimensional problem can be simplified into a two-dimensional problem. This study adopted the models of sand and clay in conjunction with the commercial software *FLAC*^{2D} [19] to simulate ground movements induced by the driving of a PC pile. After simulating the ground movements, this study investigated the load-displacement behavior of driven PC piles in silty sand.

FLAC^{2D} software [19] has a built-in function called *FLACish* language for user-owned constitutive models. This study used *FORTRAN* language to establish a preprocessor for greater effectiveness and to avoid input errors. When users input the basic parameters into the program, such as the pile length, diameter, thickness of soil layers, relative density of sand and/or undrained strength of clay, the stand-alone program was performed to obtain an output file in the *FLACish*-style language; thereafter, the output file was called into the *FLAC*^{2D} program to execute the numerical analysis for piles. As shown in Fig. 4, because there are 11 soil layers in the stratum, this study established 11 constitutive models for sand and clay in the *FLAC*^{2D} program. After that, the *FLAC*^{2D} performed the numerical analysis of ground movements induced by the driving of a PC pile.

The numerical analysis in this study involved making the following assumptions:

1. The pile body is elastic and homogeneous, with Young's modulus E of 22.8 GPa and a Poisson ratio ν of 0.17.
2. The soil parameters are listed in Tables 2 and 4; the interface parameters are listed in Table 5.
3. The driven pile exhibits axial symmetry.
4. The ground movements caused by pile driving can be simulated using a series of pseudo-static simulations, as described in the next section.
5. After the pile-driven has been simulated, the displacement is uniformly applied to the top of the driven pile to analyze the load-displacement behavior of piles.

Wang [27] performed a series of numerical studies to in-

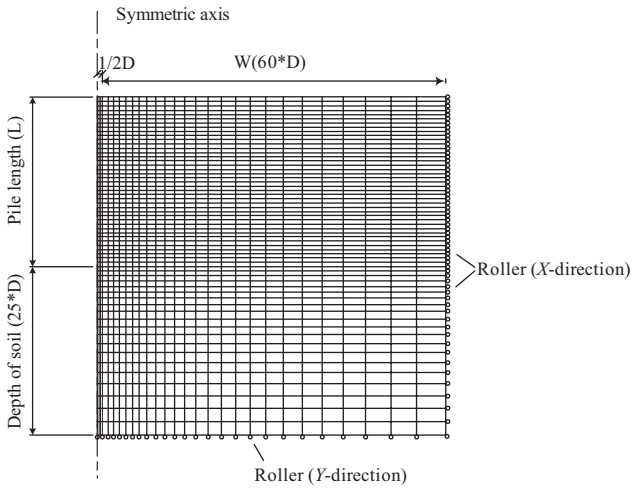

Fig. 5. Typical mesh density used for the numerical analysis (D = 0.5 m, L=10 m).

vestigate the boundary effects on analyzing driven piles, concluding that a distance of 60D between the pile and the side boundary and a net distance of 25D between the pile base and the bottom boundary are appropriate for analyses. Hence, as Fig. 5 shows, a distance of 60D between the pile and the side boundary and a net distance of 25D between the pile base and the bottom boundary were maintained to minimize the boundary effects.

According to Bowles [4], Eq. (4) yields the relationship between the relative density D_r of sand and the number of *SPT* blows, N.

$$D_r = 0.05 + 0.017N \tag{4}$$

The *SPT* blow count was obtained while investigating the site. However, the *SPT-N* value must be corrected to a standard value of effective overburden stress σ_v' (100 kN/m^2). The relative density was then estimated using Eq. (4). Consequently, the parameters required for the sand model are shown in Table 2, based on the relative density. Because the test site where the PC pile is driven into the ground includes sand and clay, the constitutive model of clay was also required for numerical analysis. Eq. (5) shows the relationship between the undrained shear strength S_u and the *SPT-N* value [4].

$$S_u = 5.0 \times N \quad (kPa) \tag{5}$$

Once the N value is known, the undrained shear strength can be calculated using Eq. (5). Accordingly, the clay parameters required for numerical analysis are shown in Table 4, based on the undrained shear strength.

A series of numerical tests was performed to simulate the driving of a PC pile (D= 80 cm, L= 34 m). Based on the results of these tests, this study recommends a reasonable procedure for estimating ground movement (Fig. 6).

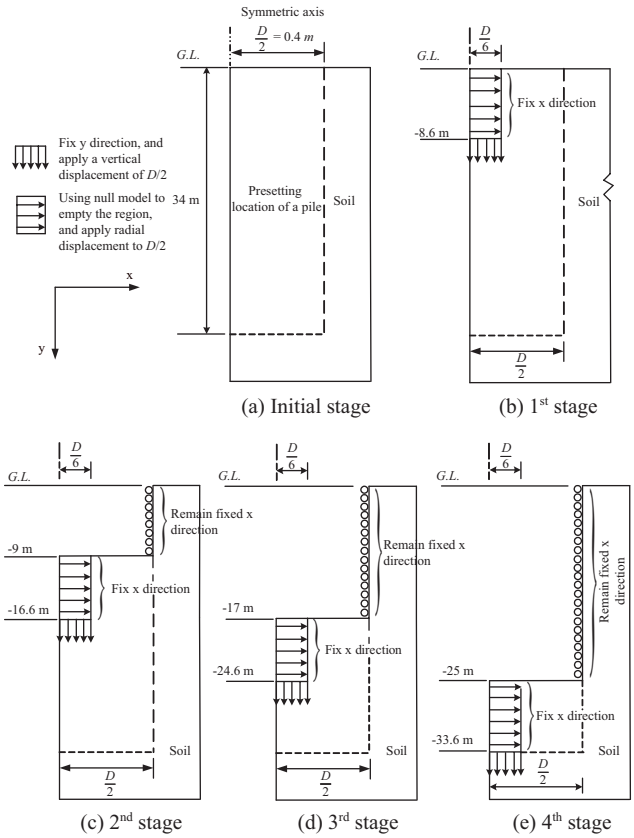

Fig. 6. Schematic diagrams of the numerical simulating process of the pile being driven into subsoil in the Chiayi-Taibao City.

1. Draw the numerical mesh and pre-specify the pile location (Fig. 6(a)).
2. Simulate the first driving stage (Fig. 6(b)): (1) In the range of boundaries from the ground surface to a *G.L.* of -8.6 m, the X directions of the nodes at a radial distance of D/6 from the symmetric axis should be fixed. (2) At a *G.L.* of -8.6 m, the Y directions of the nodes from the symmetric axis to D/6 should be fixed. (3) Empty the space at radial widths of 0 to D/6 and vertical lengths of *G.L.* 0 to -8.6 m. (4) Apply a radial displacement to D/2 to the nodes with fixed X directions. This process increases the pile radius to D/2. Meanwhile, apply a vertical displacement of D/2 to the nodes of which the Y directions are fixed. This step involves simulating the driving of a pile into the ground to the desired depth of 9 m.

The following discussion explains these procedures. Theoretically, to simulate a PC pile during driving, the radical displacement should be applied from the symmetric axis to D/2. However, each point on the symmetric axis is a singular point, and applying any displacement or stress on these points is impossible. This study attempted to apply radical displacement from D/8 to D/2; consequently, the numerical results show that the ground movements were extremely similar to those of applying radical displacement from D/6 to D/2. In addition, because the PC pile tip is

Table 6. Pile characteristics and soil properties.

Site name and reference	Pile No.	Equivalent Diameter (cm)	Length (m)	Pile Type	Soil properties
Site 1 Keelung River (This study)	1	60	27	Prestressed concrete pile	ϕ = 35.4°, γ= 18.50 kN/m^3 *GWT* at *GL*. -1 m
	2	60	27		
Site 2 Arkansas River (Mansur and Huter [21])	1	41	16	Concrete pile	ϕ = 32°, γ= 15.40 kN/m^3 *GWT* at *GL*. -0.7 m
	2	51	16		
Site 3 Tigris River (Altaee *et al.* [2])	1	35	11	Square concrete pile, B = 28.5 cm	ϕ = 34°, γ= 18.06 kN/m^3 *GWT* at *GL*. -6 m
	2	35	15		

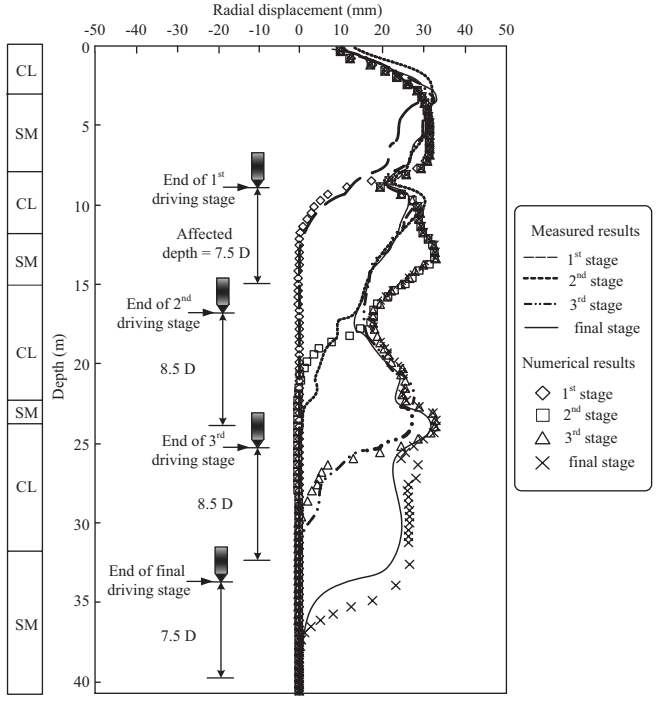

Fig. 7. Comparison of measured and modeled radial ground movement at a distance of 3*D* (2.4 m) from the center of the pile (Note: the measured results were redrawn from Hwang *et al.* [18]).

conical and has an included angle of 45° with a vertical line, geometric conditions mean that if the radical displacement is *D*/2, the vertical displacement is also *D*/2 as the PC pile is being driven.

3. As Figs. 6(c)-6(e) illustrate, the processes for simulating the second, third, and final driving stages are similar to Step 2 in simulating the first driving stage. Finally, the pile tip comes to rest at *G.L.* -34 m.

This study compared the numerical results with actual measurements [18]. Fig. 7 shows that most of the numerical results for each driving stage were similar to those measured using the inclinometer, except at *G.L.* of -12 m to -15 m. The numerical study showed that as the sandy deposit located at *G.L.* of -12 m to -15 m was changed into a clayed deposit, additional compatible curves were found. Fig. 7 also shows that the radial movement in a sandy layer exceeded that in a clay layer, possibly because of sand dilation during shearing.

Because the discrepancy between most of the numerical analyses and the field tests was small, the same procedure was adopted to simulate the driving of piles for other dimensions. After simulating the driving process of the pile, the empty region was replaced by a PC pile body. The interface elements were also employed. Pile meshes and stresses in these elements were regenerated before repeating the *FLAC*^{2D} program. After the stresses were balanced, incremental displacements were applied to the top of the pile to examine the axially loaded behaviors of driven PC piles in sandy soil.

V. CONFIRMING NUMERICAL RESULTS

To confirm the suitability of the proposed model for analyzing the load-displacement behavior of driven PC piles in sandy soil, this study compared the calculations with the results of the pile load tests in the Taipei Basin and the pile load test results presented in two previous studies [2, 21]. Table 6 shows information for three test sites. According to the investigation of Site 1, the subsoil along the Keelung River in the Taipei Basin typically consists of alternating layers of silty sand and silt. The average *SPT-N* value is 17. The friction angle ϕ of 35.4° (under the condition of confining pressure σ_3 = 1 atm) was adopted in this study. The ground water table was located at *G.L.* -1 m. Two PC piles at Site 1 exhibit the same dimensions, a diameter of 60 cm and a length of 27 m. Site 2 is near the Arkansas River [21], where the subsoil consists of poorly graded sand and silty sand. The friction angle is ϕ = 32°, the ground water table is located at *G.L.*-0.7 m, and two PC piles have diameters of 41 cm and 51 cm and the same length of 16 m. Site 3 nears the Tigris River [2]; the tested stratum consists of clayey silty sand, silty sand, and a thick layer of uniform sand. The average friction angle is ϕ = 34°, and the ground water table is located at *G.L.*-6 m; two square concrete piles have the same width of 28.5 cm and lengths of 11 m and 15 m. This analysis involved using an equivalent diameter of 35 cm.

Figs. 8-10 depict the load-displacement behavior of both field tests and numerical results for all six driven piles at the

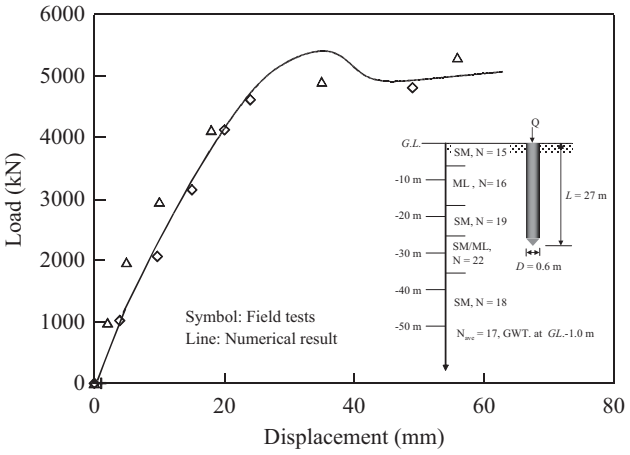

Fig. 8. Comparison of measured and calculated load-displacement curve of driven *PC* piles along the bank of Keelung River in the Taipei Basin.

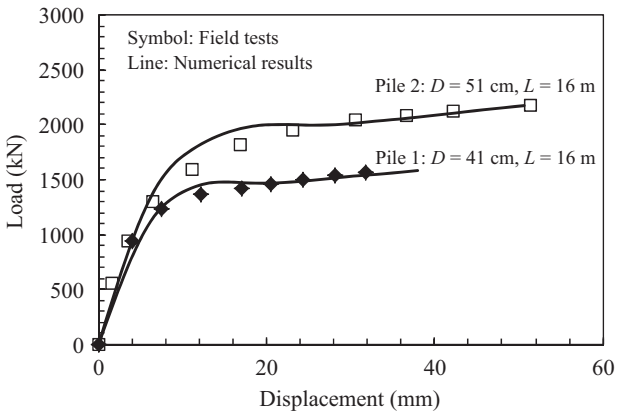

Fig. 9. Numerical and measured load-displacements of two Arkansas River piles (Note: the measured results were redrawn from Mansur and Hunter [21]).

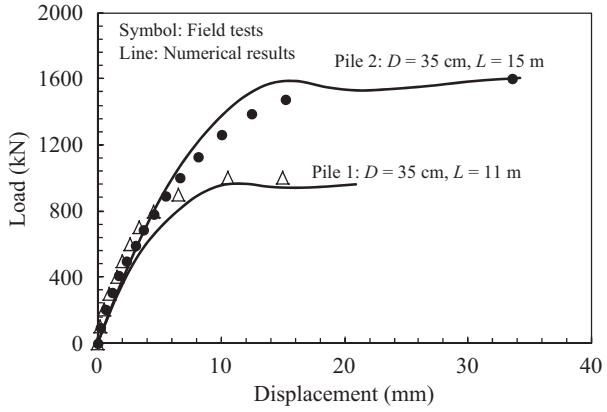

Fig. 10. Numerical and measured load-displacements of two Tigris River piles (Note: the measured results were redrawn from Altaee *et al.* [2]).

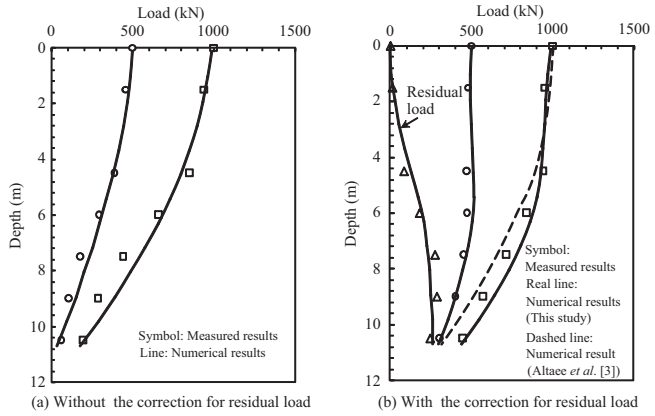

Fig. 11. Numerical and measured load transfer of the Tigris River pile 1 (Note: the measured results were redrawn from Altaee *et al.* [2]).

three test sites. These figures indicate that the numerically calculated load-displacement curves were close to those measured in the field tests. However, when the applied load was close to its peak value, an inconsistency emerged between the load-displacement curve obtained from the field tests and those obtained numerically. This was caused by applying incremental loads to the tested pile and subjecting incremental displacements to the simulated pile. However, because the proposed model considers the strain-softening behavior of soil, the post-peak behavior of a driven pile can be calculated. This study analyzed the load transfer within the pile shaft recorded by Altaee *et al.* [2], as shown in Fig. 11. Irrespective of whether the load transfer was corrected for the residual load, the numerically analyzed load transfer along the pile shaft was in good agreement with that measured from field tests. In addition, compared with the analytical results obtained by Altaee *et al*. [3], the load transfers analyzed in this study were closer to the field results.

VI. PARAMETTIC STUDY

After verifying the proposed method by using field test results, this study used the proposed method to elucidate the effects of the following parameters on the behavior of axially loaded driven PC piles in silty sand: (1) relative density of silty sand (D_r = 30% and 70%); (2) pile diameter (D = 0.5 m, 0.6 m, 0.8 m, and 1.0 m); and (3) pile length (L = 10 m, 20 m, and 30 m). All piles, both driven and loaded, were analyzed.

1. Load-Displacement Behavior of a Driven PC Pile

Researchers typically regard the post-load-displacement behavior of a pile as the peak-load-displacement behavior. Nevertheless, the friction force and end bearing do not reach their peak values simultaneously. Generally, when the shaft friction reaches its peak value, the end bearing is still small; when the end bearing develops, the shaft friction is in a residual state. Furthermore, a residual load around the pile shaft is generated when a pile is driven. Fig. 12 plots the load-displacement behavior of a PC pile with a diameter D of 0.5 m

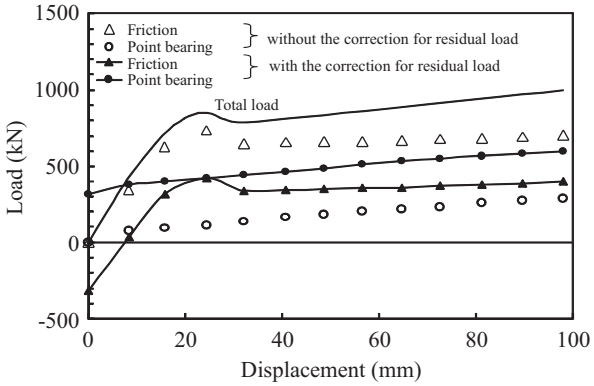

Fig. 12. Load-displacement curve of a driven PC pile (D = 0.5 m, L = 10 m, D_r = 30%).

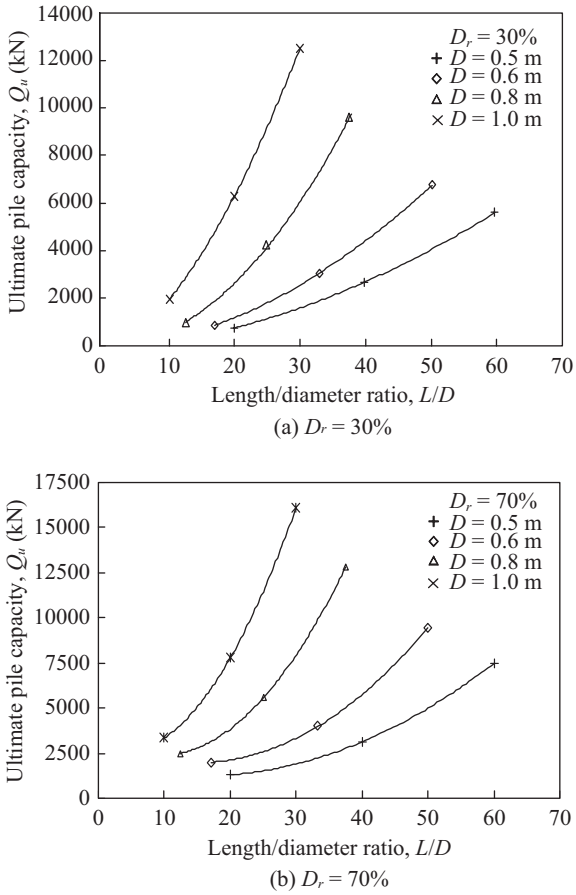

Fig. 13. Relationships between the ultimate pile capacity and length/diameter ratio L/D for various pile diameters and various relative densities of silty sand.

and length L of 10 m, which is driven into silty sand with a D_r of 30%. This figure shows that the shaft friction and the point bearing corrected for the residual load differed from those without correction for the residual load. For curves with the correction for the residual load, the initial end bearing was positive, whereas the initial shaft friction was negative. Remarkably, the total load, with or without the correction of the residual load, was the same. Fig. 12 also demonstrates that the total load increased rapidly with the pile displacement initially, and the total load peaked at a displacement of approximately 4% D. The shaft friction also initially increased rapidly with pile displacement, and fell from its peak to the residual value. The residual shaft friction developed to a steady state that corresponded to a pile displacement of approximately 6% D. By contrast, the point bearing slowly increased continuously without a peak. Consequently, the total load initially declined and then increased with the pile displacement at the post-peak stage. For ease of comparison with the ultimate capacities of the piles, this study defined the first peak load as the ultimate capacity. However, Fig. 12 shows that the proposed model effectively elucidated the post-peak behavior of a pile.

2. Parametric Effects on Ultimate Capacity of Driven PC Piles

After a series of parametric investigations, this study briefly summarized the numerical studies on the pile diameter, pile length, and relative density of sand to elucidate the effect of these parameters on the ultimate pile capacity. Fig. 13 shows that the ultimate pile capacity increased with the pile length/diameter ratio L/D, and no critical depth could be found in this study. A larger diameter was associated with a greater increment in the ultimate load; in addition, the ultimate pile capacity increased with the relative density of the sand. However, as the relative density changed from 30% to 70%, the ultimate pile capacity increased by only 20% because the pile driving results in condensing loose sand and dilating dense sand.

Researchers in Taiwan have accumulated dozens of pile test results. This study gathered results from the reclaimed site at Mailiao Industrial Park, Yun-Lin County and the bank along the Keelung River in the Taipei Basin in Taiwan, where the tested pile displacement exceeds 0.10 D. Subsequently, this study used the method proposed by Terzaghi [25] to estimate the ultimate pile capacity for comparison with the numerical results. The soil in Yun-Lin County and the Taipei Basin have alternating layers of silty sand and silt, with *SPT-N* values ranging from 15 to 22. Thus, Eq. (4) obtains a relative density D_r of approximately 30%-42%. Fig. 14 shows that the discrepancy between the numerical results and the field results was small not only for the driven PC pile with D = 0.5 m, but also for that with D = 0.6 m. Therefore, the data shown in Figs. 13 and 14 are helpful for designing driven PC piles, especially for large-scale piles.

VII. CONCLUSION

This study developed a numerical method for investigating the ground movements of a large-scale PC pile driven deeply into a stratum of multiple layers. Results obtained in situ concerning driven piles were applied to confirm the reliability of the proposed numerical approach. This study also performed parametric studies, drawing the following conclusions:

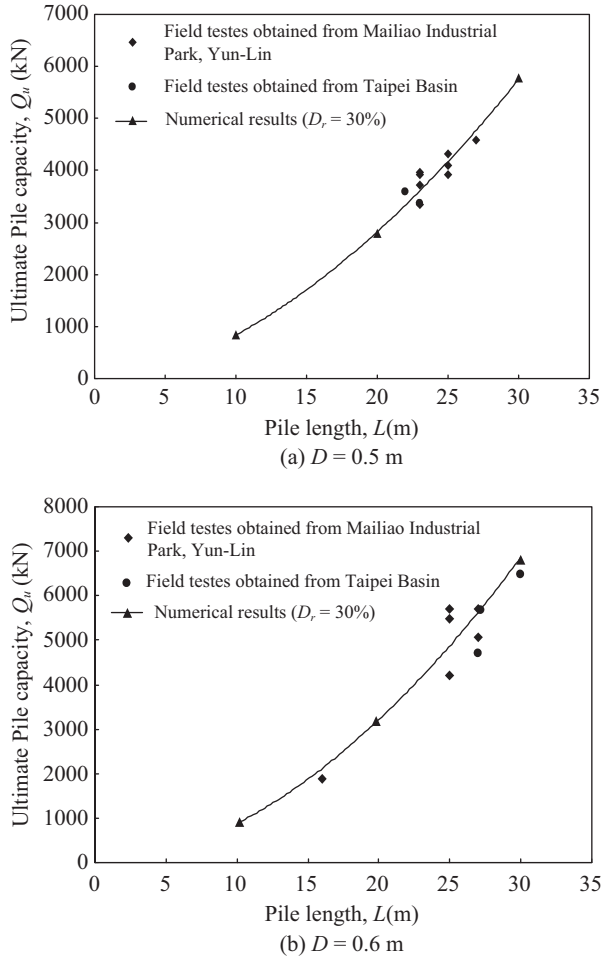

Fig. 14. Comparison of the measured and the calculated ultimate load that developed with pile length for different pile diameters.

1. The model used by the author cannot simulate the stress reversal and stress concentration around a pile between hammer strokes. However, the radial ground movement and residual load caused by driving a pile can be simulated and analyzed using the proposed method.
2. The numerically calculated load-displacement curves of the piles with different dimensions in various strata of sandy soils were consistent with those measured in situ tests.
3. Because in situ loading on a PC pile differs from that modeled numerically, the post-peak behaviors estimated by performing field tests differed from those analyzed numerically. However, the proposed numerical method identified the post-peak behavior of a pile.
4. Total load, shaft friction, and point bearing did not reach their peak values simultaneously. Shaft friction declined as pile displacement increased at the post-peak stage. No peak point bearing appeared when the pile was stressed. The residual load induced by driving a PC pile significantly affected the behaviors of the shaft friction and end bearing of a driven pile.
5. The ultimate load increased with the pile diameter and with the pile length, and no critical depth can be determined. However, the ultimate load increased by only 20% when the relative density of sand changed from 30% to 70% because the pile driving resulted in condensing loose sand and dilating dense sand. This study presents useful figures for designing a PC pile, particularly a large-scale driven PC pile.

ACKNOWLEDGMENTS

The authors would like to thank the National Science Council of the Republic of China, Taiwan, for financially supporting this research under Grant No. NSC 99-2628-E-324-005. The authors also appreciate Professor Hwang, J. H. of National Central University, Professor Chen, C. H. of National Taiwan University, and Mr. Yeh, W. C. of Resources Engineering Services Inc., for providing a tremendous amount of information on pile driving, and Mr. Hung, C. J., and Mr. Chen, C. K., of Da-Chen Construction and Engineering Corp. for helping with the installation and testing of the test piles.

REFERENCES

1. Alawneh, A. S., Nusier, O., Husein Malkawi, A. I., and Al-Kateeb, M., "Axial compressive capacity of driven piles in sand: a method including post-driving residual stresses," *Canadian Geotechnical Journal*, Vol. 38, No. 2, pp. 364-377 (2001).
2. Altaee, A., Fellenius, B. H., and Evgin, E., "Axial load transfer for piles in sand. I. Tests on an instrumented precast pile," *Canadian Geotechnical Journal*, Vol. 29, No. 1, pp. 11-20 (1992).
3. Altaee, A., Fellenius, B. H., and Evgin, E., "Axial load transfer for piles in sand. II. Numerical analysis," *Canadian Geotechnical Journal*, Vol. 29, No. 1, pp. 21-30 (1992).
4. Bowles, J. E., *Foundation Analysis and Design*, 5th Edition, McGraw-Hill (1996).
5. Briaud, J. L. and Tucker, L., "Piles in sand: a method including residual stresses," *Journal of Geotechnical Engineering Division*, Vol. 110, No. 11, pp. 1666-1680 (1984).
6. Burland, J. B., "Shaft friction of piles in clay--a simple fundamental approach," *Ground Engineering*, Vol. 6, No. 3, pp. 30-42 (1973).
7. Chan, S. F. and Hanna, T. H., "Repeated loading on single piles in sand," *Journal of the Geotechnical Engineering Division*, Vol. 106, No. 6, pp. 171-188 (1980).
8. Chen, C. H., Perng, T. D., Hwang, J. H., and Chang, L. T., "Analyses for load test data of PC piles on west-coast reclaimed areas of Taiwan," *Journal of the Chinese Institute of Civil and Hydraulic Engineering*, Vol. 12, No. 1, pp. 29-40 (2000).`
9. Desai, C. S., Zaman, M. M., Lightner, J. G., and Siriwardane, H. J., "Thin-layer elements for interfaces and joints," *International Journal for Numerical and Analytical Methods in Geomechanics*, Vol. 8, No. 1, pp. 19-43 (1984).
10. Guo, P., "Numerical modeling of pipe-soil interaction under oblique loading," *Journal of Geotechnical and Geoenvironmental Engineering*, Vol. 131, No. 2, pp. 260-268 (2005).
11. Hanna, T. H. and Tan, R. H. S., "The behavior of long piles under compressive loads in sand," *Canadian Geotechnical Journal*, Vol. 10, No. 3, 311-340 (1973).
12. Holloway, D. M., Clough, G. W., and Vesic, A. S., "The effects of residual driving stresses on pile performance under axial load," *Proceedings, 10th Offshore Technology Conference*, Houston, Vol. 4, pp. 2225-2236 (1978).
13. Hsu, S. T., "A constitutive model for uplift behavior of anchors in cohe-

sionless soils," *Journal of the Chinese Institute of Engineers*, Vol. 28, No. 2, pp. 305-317 (2005).
14. Hsu, S. T., "Numerical simulation of driven piles in alluvial soil," *Applied Mechanics and Materials*, Vols. 105-107, pp. 1415-1419 (2011).
15. Hsu, S. T., "Axially loaded behavior of driven PC piles," *AIP Conference Proceedings*, Vol. 1233, pp. 1511-1506 (2010).
16. Hsu, S. T. and Liao, H. J., "Uplift behavior of cylindrical anchors in sand,"*Canadian Geotechnical Journal*, Vol. 35, No. 1, pp. 70-80 (1998).
17. Hsu, S. T., Lin, S. Y., and Hung, C. J., "Analyses for axially loaded behavior of prestressed concrete piles," *Journal of the Chinese Institute of Civil and Hydraulic Engineering*, Vol. 19, No. 1, pp. 13-23 (2007).
18. Hwang, J. H, Liang, N., and Chen, C. H., "Ground response during pile driving," *Journal of Geotechnical and Geoenvironmental Engineering*, Vol. 127, No. 11, pp. 939-948 (2001).
19. Itasca Consulting Group Inc., *FLAC: Fast Lagrangian Analysis of Continua*, Version 3.3, Vol. 1-4, Minnesota (1996).
20. Lin, Y. H., *Uplift Behavior of Shaft Tension Anchors in a Layer Soil*, Master Thesis, Department of Construction engineering, Chaoyang University of Technology, Taichung (2005).
21. Mansur, C. I. and Hunter, A. H., "Pile tests: Arkansas River project," *Journal of Soil Mechanics and Foundation Engineering Division*, Vol. 96, No. SM5, pp. 1545-1582 (1970).
22. Nicola, A. D. and Randoph, M. F., "Tensile and compressive shaft capacity of pile in sand," *Journal of Geotechnical Engineering Division*, Vol. 119, No. 12, pp. 1952-1973 (1993).
23. Poulos, H. G., "Analysis of residual stress effects in piles," *Journal of Geotechnical Engineering*, Vol. 113, No. 3, pp. 216-229 (1987).
24. Said, I., Gennaro, V. D., and Frank, R., "Axisymmetric finite element analysis of pile loading tests," *Computers and Geotechnics*, Vol. 36, No. 1, pp. 6-19 (2009).
25. Terzaghi, K., "Discussion on the progress report of the Committee on the Bearing Value of Pile Foundations," *Journal of Soil Mechanics and Foundation Engineering Division*, Vol. 68, No. 2, pp. 311-323 (1942).
26. Trochanis, A. M., Bielak, J., and Christiano, P., "Three-dimensional nonlinear study of piles," *Journal of Geotechnical Engineering Division*, Vol. 117, No. 3, pp. 429-447 (1991).
27. Wang, J. L., *A Study on the Axial Loaded Behavior of Driven Prestressed Concrete Piles*, Master Thesis, Department of Construction Engineering, Chaoyang University of Technology, Taichung, Taiwan (2007).